

Electro-Optic Sampling of a Free-Running Terahertz Quantum-Cascade-Laser Frequency Comb

Sergej Markmann[✉], David Stark, Matthew Singleton, Mattias Beck, Jérôme Faist, and Giacomo Scalari

Institute for Quantum Electronics, ETH Zürich, Auguste-Piccard-Hof 1, Zürich 8093, Switzerland

(Received 5 July 2022; revised 28 March 2023; accepted 25 May 2023; published 21 June 2023)

Quantum-cascade-laser (QCL) frequency combs are compact semiconductor light sources operating in the mid-IR and terahertz frequencies. Achieving subpicosecond laser pulses with high peak power is of vital importance for performing nonlinear time-resolved spectroscopy as well for exploring nonlinear phenomena. Therefore, investigation and characterization of time-resolved free-running laser emission is a key for further improvement and optimization of these intersubband devices. In this work, we demonstrate a direct electric field measurement of a free-running terahertz QCL frequency comb using electro-optic sampling in combination with computational phase correction, where we retrieve the electric field profile and access the comb parameters. The demonstrated method is of high interest for time-resolved low-power laser emission characterization, typical for ring terahertz QCL frequency combs and investigation of phase-compensated emission via waveguide dispersion engineering for broadband comb operation.

DOI: 10.1103/PhysRevApplied.19.064063

I. INTRODUCTION

Recent progress in the field of quantum cascade lasers (QCLs) has gained a lot of attraction with regard to the time-resolved demonstration of subpicosecond QCL pulses [1] and the formation of solitons in ring QCLs [2] in the mid-IR. Because of the similarity between mid-IR and terahertz QCLs, the generation of dissipative Kerr solitons is also feasible in ring terahertz QCLs [3]. Dispersion engineering in waveguides is also of vital importance, which requires phase information about individual modes. Therefore, it is of great technological interest to develop time-resolved techniques for direct electric field measurement of free-running low-power terahertz QCL frequency combs and to access the parameters underlying these combs.

In the last decade, three different approaches have been developed with the goal either to measure directly or to reconstruct the electric field profile of QCLs. The first to be discussed is a dual-comb (DC) spectroscopy technique [4,5], which utilizes two frequency-comb lasers with overlapping spectra and slightly different repetition rates [6–8]. Considering one of the frequency combs as fully characterized, the temporal field profile of the second comb can be reconstructed from the recorded multiheterodyne signal (interferogram) [9]. Recently, also a fully phase-stabilized terahertz QCL frequency comb was demonstrated using this approach [10]. However, field reconstruction with this

method relies on active stabilization schemes [7,11] and hence it is not applicable to a free-running laser.

In the case of two free-running frequency-comb lasers, the resulting spectrum of the multiheterodyne signal is broadened due to the temporal fluctuation of repetition rates and the carrier-envelope offsets of both lasers. In order to add the acquired interferograms coherently, computational phase-correction algorithms have to be used [12–14]. In Ref. [12] the dual-comb interferogram was fitted to the frequency-comb model with the help of the extended Kalman filter, and later in Ref. [13] a generalized computational method was introduced for phase corrections employing an augmented Kalman filter. One of the difficulties of the Kalman-filter approaches is that they require knowledge of amplitude and phase noise correlation matrices, which has to be estimated or measured [15]. The final result of the least-squares fit could still be one of the local minima of the merit function. In contrast to these techniques, the computational coherent averaging (CoCoA) algorithm [14] does not require any additional information, nor any fitting parameters. The method corrects the temporal fluctuation of the repetition rate and the carrier-envelope offset frequency of the recorded interferogram.

A second technique to elucidate the time-domain profile of a terahertz QCL's emission is shifted-wave interference Fourier-transform (SWIFT) spectroscopy [16,17]. The main idea of the framework reported in Ref. [16] is a direct measurement of the phase differences of the neighboring comb modes. With the knowledge of the measured

* msergej@phys.ethz.ch

phase differences, the electric field profile is reconstructed. Unfortunately, time-resolved field reconstruction on millisecond or microsecond time scales is challenging with this method, as sufficiently fast and simultaneously high-spectral-resolution FT spectrometers are currently unavailable. This makes observation of frequency-comb dynamics on microsecond and millisecond time scales impossible, which would be of high interest, since the noise contribution in QCLs is significantly modified at acquisition speed below milliseconds [18]. However, with the recently developed frequency-chirped Fourier-transform spectroscopy [19], which exploits a rotational optical delay line, SWIFT spectroscopy on submillisecond time scales is within reach.

The third approach is based on electro-optic (EO) sampling [20]. Two different techniques employing EO sampling have emerged independently from each other, namely the phase-seeding [21] and phase-locking [22] techniques. In the case of phase seeding, a broadband seed pulse is injected into the QCL cavity, originating typically from a photoconductive terahertz antenna [23,24], a spintronic emitter [25,26] or a nonlinear crystal [27,28]. As soon as the seed enters the laser cavity, the QCL is biased with synchronized nanosecond radio-frequency (rf) pulses above the laser threshold. In this way, the phases of the seed are imprinted on the QCL emission, which results in an actively mode-locked laser with coherent terahertz emission [29,30]. This method also supports non-frequency-comb operation. The phase-seeding technique has been successfully utilized for terahertz pulse amplification [31], laser emission control [32,33], terahertz pump-probe spectroscopy [34], two-dimensional spectroscopy of biased and nonbiased quantum-cascade lasers and structures [35–37], and terahertz pulse compression [38]. On the other hand, the phase-locking method requires a terahertz frequency comb. In combination with a stabilized repetition rate $f_{\text{rep}}^{\text{QCL}}$, via the rf injection [39], and stable carrier-envelope offset frequency ($f_{\text{ceo}}^{\text{QCL}}$), ensured by direct current feedback with a phase-lock loop [40], active mode locking is achieved [41]. This allows coherent acquisition of the terahertz electric field.

All the above-described approaches and methods, with the exception of the SWIFT technique, require an actively mode-locked terahertz QCL in order to directly measure the electric field of the laser on submicrosecond time scales. In contrast, SWIFT can be applied to free-running lasers, but it reconstructs an averaged signal and does not directly measure the electric field. Thus, there are currently no available methods to directly measure the electric field of a free-running terahertz QCL on submicrosecond time scales.

In this work we address this question and demonstrate the time-resolved electric field measurement of a free-running terahertz QCL frequency comb using an

EO-sampling technique in combination with a computational phase-correction algorithm. By employing the digital postprocessing technique, we are able now to extract the phases of a free-running laser, which is not possible in the traditional way, by employing the rf stabilization technique (mode locking), which might perturb the comb state. Although, a free-running femtosecond laser is employed for EO sampling, no information about the femtosecond laser is required for the reconstruction of the terahertz QCL electric field on microsecond time scales beyond its repetition rate because EO sampling relies on the periodicity of the intensity envelope of the femtosecond pulses and not their individual phases.

II. RESULTS

A. Experimental setup

The experimental setup of the system is shown in Fig. 1(a). One of the frequency combs utilized in this work is a commercial Ti:sapphire femtosecond laser with repetition rate ($f_{\text{rep}}^{\text{fs}}$) of 79.64 MHz and a carrier frequency centered at 800 nm (374 THz). The second frequency comb is a terahertz QCL with $f_{\text{rep}}^{\text{QCL}} \sim 15.377$ GHz and lasing center frequency $\nu^{\text{QCL}} = 1.84$ THz. The beam of the terahertz QCL is spatially overlapped with the femtosecond-laser beam with the help of parabolic mirrors. Both beams are focused onto a 2-mm-long birefringent ZnTe crystal. Because of the Pockels effect in the ZnTe crystal and the combination of $\lambda/4$ wave plate, Wollaston prism (WP), as well as a fast balanced-photodiodes assembly, the polarization state of individual femtosecond-laser pulses can be analyzed. The signal output from the balanced photodiodes is proportional to the incident terahertz electric field [42]. The acquisition is synchronized with the femtosecond laser, which is realized by using the electrical clock signal of the femtosecond laser as the external sampling clock for the acquisition card. For ensuring a sufficient signal-to-noise ratio (SNR), it is of vital importance to extract the entire terahertz radiation emitted into free space from the laser facet and tightly focus it onto the ZnTe crystal. The active region is embedded into a metal-metal waveguide, which ensures better comb stability and temperature performance.

The disadvantages of this waveguide are a low outcoupling efficiency and high beam divergence. To overcome these drawbacks, the radiation extraction is realized with a hemispherical silicon lens [Figs. 1(b) and 1(c)], which simultaneously serves the purpose to fit the numerical aperture of the first 3-inch parabolic mirror. The resulting far-field profile is shown in Fig. 1(d) and the light-current-voltage (L - I - V) characteristic in Fig. 2(a). The terahertz QCL is operated in continuous-wave (CW) mode in a comb regime with the corresponding spectrum shown in Fig. 2(b), as recorded with an FT spectrometer (Bruker

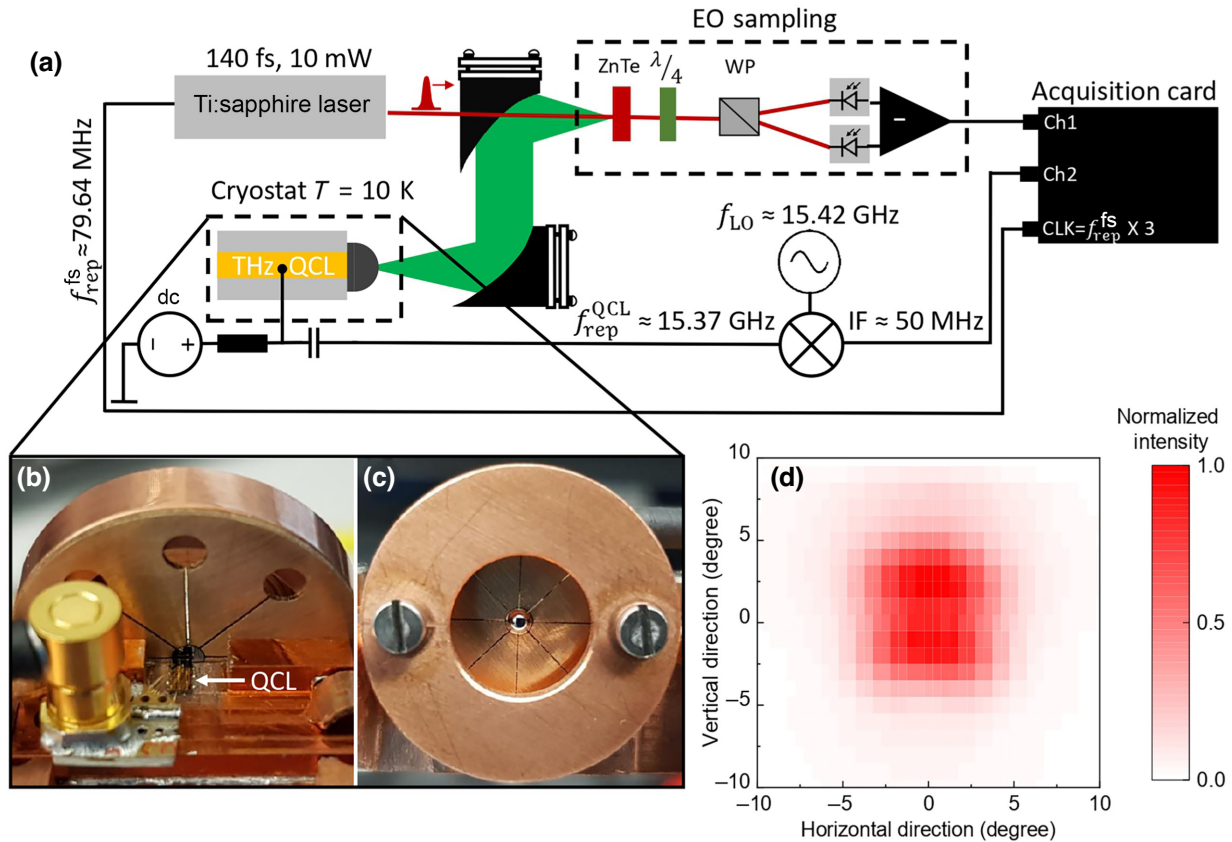


FIG. 1. (a) Schematics of the experimental setup for performing the electro-optical sampling of a free-running terahertz QCL. (b),(c) Back and front views, respectively, of the QCL with the mounted hemispherical lens arrangement for terahertz beam extraction and collimation. (d) Intensity far-field profile of the terahertz QCL with the silicon lens mounted.

VERTEX 80V). Additionally, the down-mixed intermodal beat note signal $f_d(t)$ is recorded.

B. EO sampling

Since we perform EO sampling on a free-running terahertz QCL frequency comb, a general description of the electric field of a frequency comb in the optical domain is given by the following expression [41]:

$$E(t) = e^{i2\pi\nu^{\text{QCL}}t} \sum_{m=-q}^{m=p} A_m e^{i(2\pi m f_{\text{rep}}^{\text{QCL}} t + \phi_m)} + \text{c.c.}, \quad (1)$$

where ν^{QCL} is the QCL central mode frequency, q and p are the modes below and above the central mode, A_m is the amplitude of the mode m , $f_{\text{rep}}^{\text{QCL}}$ is the repetition rate, and ϕ_m is the phase associated with the m th mode. The signal $E(t)$ is sampled with the femtosecond-laser pulses at repetition rate $f_{\text{rep}}^{\text{fs}}$; hence the EO-sampled signal is expressed as

$$E_s(t) = E(t) \sum_{k=-\infty}^{k=\infty} \delta \left(t - \frac{k}{f_{\text{rep}}^{\text{fs}}} \right). \quad (2)$$

Expanding the delta distribution in a Fourier series,

$$\delta \left(t - \frac{k}{f_{\text{rep}}^{\text{fs}}} \right) = f_{\text{rep}}^{\text{fs}} \sum_{n=-\infty}^{n=\infty} \exp(i2\pi n f_{\text{rep}}^{\text{fs}} t),$$

results in the following expression for the sampled electric field:

$$E_s(t) = e^{i2\pi\eta t} \sum_{m=-q}^{m=p} A_m e^{i(2\pi m \Delta f_{\text{rep}} t + \phi_m)} + \text{c.c.} \quad (3)$$

Here, $\eta = \nu^{\text{QCL}} - r f_{\text{rep}}^{\text{fs}}$ is the frequency position of the downsampled central mode with $r = \lfloor \nu^{\text{QCL}} / f_{\text{rep}}^{\text{fs}} \rfloor$ and $\Delta f_{\text{rep}} = f_{\text{rep}}^{\text{QCL}} - s f_{\text{rep}}^{\text{fs}}$ is the repetition rate in the rf domain with $s = \lfloor f_{\text{rep}}^{\text{QCL}} / f_{\text{rep}}^{\text{fs}} \rfloor$.

By comparing Eqs. (1) and (3) it is seen that the general shape of the signal is preserved after the downsampling. The terahertz radiation of the QCL causes amplitude modulation of the near-infrared (NIR) pulses, and hence sidebands in the NIR spectrum are generated at frequencies

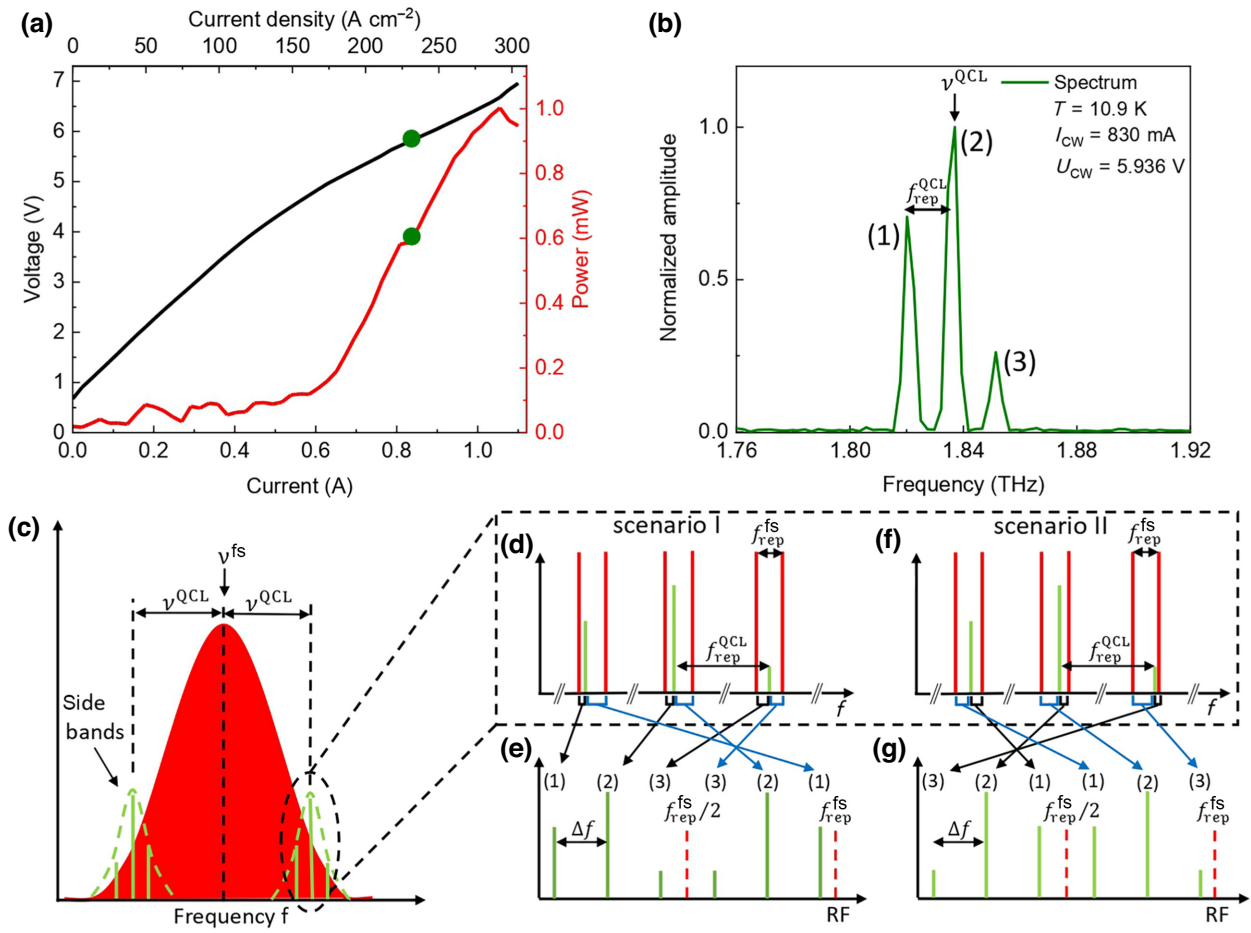


FIG. 2. (a) L - I - V characteristics of the utilized terahertz QCL in CW mode. (b) QCL spectrum taken at the operation point, which is marked with a green dot in (a). (c) Schematic femtosecond-laser spectrum (in red) with sidebands (in green), generated by the amplitude modulation with the terahertz QCL. The sideband maxima are spaced by $\pm v^{QCL}$ from the maximum of the femtosecond-laser spectrum. (d),(f) Enlarged views of the overlap region of the femtosecond-laser spectrum and the side modes. Depending on f_{rep}^{QCL} and f_{ceo}^{QCL} , these are the two arrangements of the sideband with respect to the femtosecond-laser modes that are of interest. (e),(g) Down-mixed QCL spectrum for the given mode arrangement in (d),(f).

$\pm v^{QCL}$ from the NIR spectrum maximum [Fig. 2(c)]. Each sideband contains all modes of the QCL. In the case of sufficiently short femtosecond pulses, spectral overlap between the femtosecond-laser spectrum and the generated sidebands is possible. It is important to note that the spectrum of the $E_s(t)$ signal has no $f_{\text{ceo}}^{\text{fs}}$ dependence. This is the case because the spectrum is constructed by the frequency difference between the sideband modes and the femtosecond-laser spectrum, which cancel out the $f_{\text{ceo}}^{\text{fs}}$ dependence. In the case where high-resolution (below $f_{\text{rep}}^{\text{fs}}$) spectral measurements of the terahertz QCL are carried out, the carrier frequency of the laser, and hence f_{ceo}^{QCL} , can be computed from the measured η frequency. In our case, η is afflicted with an uncertainty, due to our spectrometer resolution of several gigahertz. However, as has been recently demonstrated by employing two femtosecond lasers with slightly different repetition rates, frequency unambiguity can be achieved [43].

The relative position of the generated sidebands, with respect to the NIR spectrum, depends on f_{rep}^{QCL} and f_{ceo}^{QCL} . With the comb spectrum in Fig. 2(b), there are two possible scenarios (I and II). Because of the quadratic detection nature of the photodiodes, we measure the beating between the femtosecond-laser modes and the generated sideband modes. The resulting beating spectrum is shown in Figs. 2(e) and 2(g). In both cases [Figs. 2(e) and 2(g)] the entire information of the terahertz QCL spectrum is given within the $f_{\text{rep}}^{\text{fs}}/2$ bandwidth. The fact that each mode of the sideband beats with the neighboring modes of the femtosecond-laser spectrum results in the mirroring of beating spectra at frequencies that are integer multiples of $f_{\text{rep}}^{\text{fs}}/2$. This process continues towards higher and lower frequencies, but is experimentally limited by the detector bandwidth of around 120 MHz.

In scenario I [Fig. 2(e)] the shape of the original terahertz QCL spectrum [Fig. 2(b)] is preserved within the

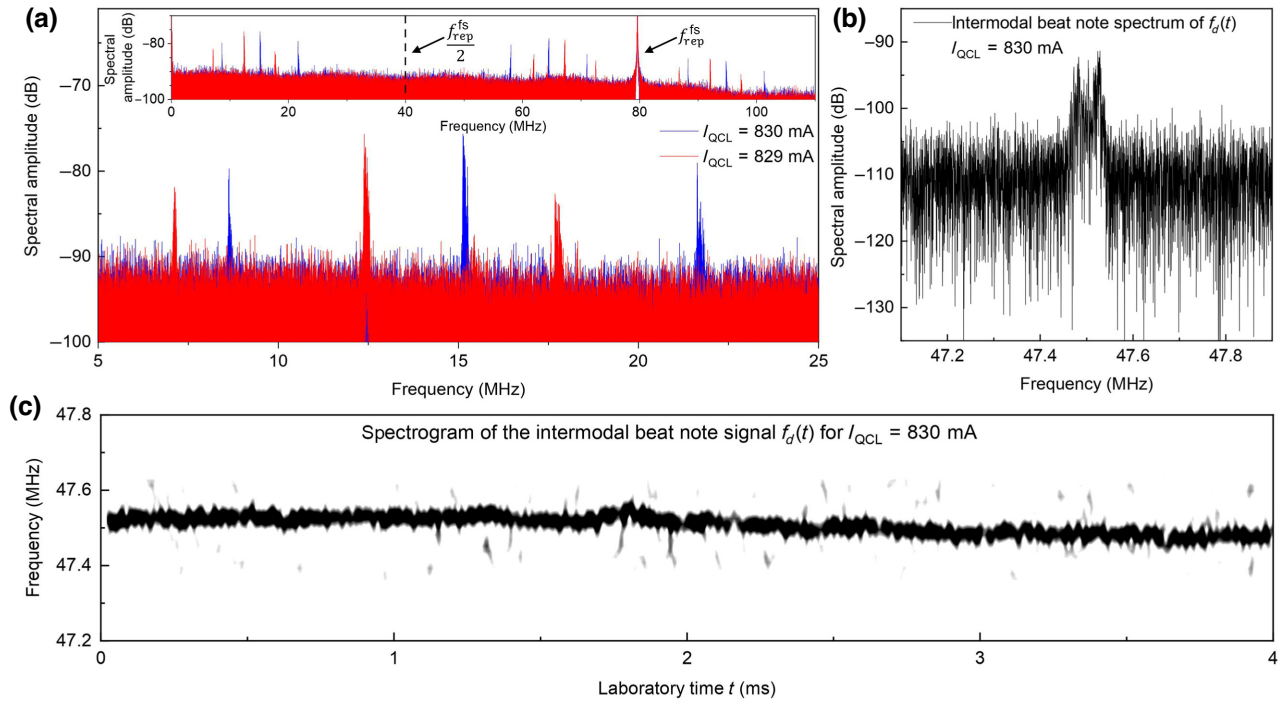


FIG. 3. (a) Spectrum of the electro-optic dual-comb signal for $I_{\text{QCL}} = 829 \text{ mA}$ (red curve) and $I_{\text{QCL}} = 830 \text{ mA}$ (blue curve). The inset shows the full spectral bandwidth covered by the balanced photodetector. (b) Down-mixed intermodal beat note signal $f_d(t)$ for $I_{\text{QCL}} = 830 \text{ mA}$. (c) Spectrogram of (b).

$f_{\text{rep}}^{\text{fs}}/2$ bandwidth, whereas in scenario II the modes m_1 and m_3 are swapped. In our system $f_{\text{rep}}^{\text{fs}}$ of the femtosecond laser is not adjustable; therefore we perform the experiment by adjusting the temperature and the current of the terahertz QCL so that the laser is in a comb regime and the resulting down-mixed QCL modes experience the same directional frequency shift for a small current change.

In order to identify which particular scenario [I or II in Figs. 2(d) and 2(f)] applies to our case, we record two interferograms at slightly different operation points. The corresponding spectra of the recorded interferograms are shown in Fig. 3(a). With increasing current, we expect the QCL modes in the optical domain to be redshifted, due to self-heating. This would result in scenario I (II) in a spectral redshift (blueshift) in the rf domain as well in the reduced (increased) repetition rate Δf_{rep} within the $f_{\text{rep}}^{\text{fs}}/2$ bandwidth. For the sake of completeness, the inset in Fig. 3(a) shows a full spectrum within the detector bandwidth (120 MHz) where mirror frequencies above $f_{\text{rep}}^{\text{fs}}/2$ and $f_{\text{rep}}^{\text{fs}}$ are present. They originate from the mixing of the sidebands with the next-neighboring femtosecond-laser mode, as has been discussed and visualized in Figs. 2(e) and 2(f). From the obtained spectra in Fig. 2(a) we clearly observe a blueshift with increasing QCL current and hence relate the mode arrangement as indicated in scenario II [Figs. 2(f) and 2(g)]. With this knowledge and without loss of generality, we can reconstruct the original temporal

electric field profile by taking the phase correction of $\Delta f_{\text{rep}}(t)$ and $f_{\text{ceo}}^{\text{QCL}}(t)$ into account.

C. Computational phase correction

Measurements are performed in the time reference of the femtosecond laser. This is realized via synchronization of the femtosecond laser and the acquisition card as shown in Fig. 1. In order to add the recorded interferogram coherently and to reconstruct the temporal evolution of the terahertz electric field, we apply computational phase correction to the recorded $E_s(t)$ signal. We first correct the temporal fluctuation of $\Delta f_{\text{rep}}(t)$ around the average value by resampling the signal $E_s(t)$ on the time axis t' given by

$$t'(t) = \sum_{i=0}^t \frac{\langle \Delta f_{\text{rep}} \rangle}{\langle \Delta f_{\text{rep}} \rangle - f_{\text{inst}}^{\text{BN}}(i)} \Delta t_s, \quad (4)$$

where $\langle \Delta f_{\text{rep}} \rangle$ is the average repetition rate of the recorded $E_s(t)$ signal and $f_{\text{inst}}^{\text{BN}}$ is the instantaneous frequency of the down-mixed beat note signal $f_d(t)$. The spectrum of the down-mixed intermodal beat note signal $f_d(t)$ is shown in Fig. 3(b) and the corresponding 4-ms-long spectrogram in Fig. 3(c), which shows a 40 kHz fluctuation.

The instantaneous frequency is extracted from the phase of the analytical signal $f_d(t)$ obtained via Hilbert transform and is shown in Fig. 4(b). We are using the $f_d(t)$

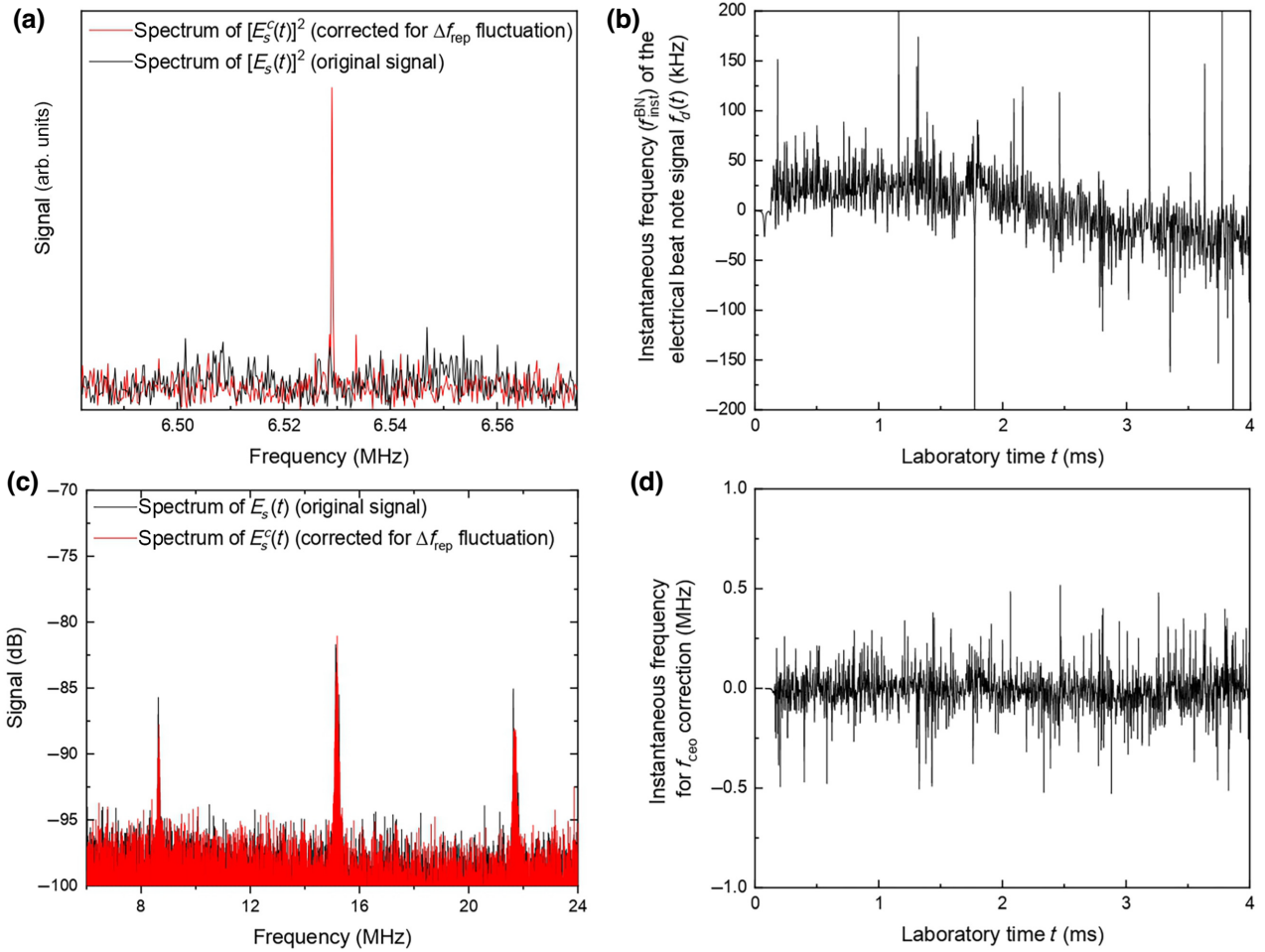


FIG. 4. (a) Computed intermodal beat note signal from the dual-comb signal for the corrected (red curve) and uncorrected (black curve) temporal Δf_{rep} fluctuation. (b) Instantaneous frequency $f_{\text{inst}}^{\text{BN}}$ extracted from the down-mixed intermodal beat note signal $f_d(t)$. (c) Spectrum of the dual-comb signal for corrected (red curve) and uncorrected (black curve) phase of Δf_{rep} . (d) Computed instantaneous frequency, which is used for the phase correction of the $f_{\text{ceo}}^{\text{QCL}}$.

signal to compute $f_{\text{inst}}^{\text{BN}}$ instead of extracting it from $E_s(t)$, because the SNR of the electrical beat note signal is higher. To verify that the resampling of the signal $E_s(t)$ on the time axis t' is realized correctly and the resulting signal $E_s^c(t)$ has a constant repetition rate, we can compute the Fourier transforms of $(E_s^c(t))^2$ and $(E_s(t))^2$ which have a signal contribution at the repetition-rate frequency as shown in Fig. 4(b). Since $\Delta f_{\text{rep}}(t)$ of the original signal has weak time dependence, this results in a broadened signal around $\langle \Delta f_{\text{rep}} \rangle = 6.528$ MHz (black curve). In contrast, the resampled signal $E_s^c(t)$ has a constant repetition rate, which is clearly visible in a localized signal at $\langle \Delta f_{\text{rep}} \rangle$ in Fig. 4(a) (red curve). Such a localized signal contribution shows that the temporal dependence of Δf_{rep} has been computationally corrected. The resulting spectra of the repetition-rate corrected signal ($E_s^c(t)$) and uncorrected signal ($E_s(t)$) are shown in Fig. 4(c). The signal $E_s^c(t)$ describes $\langle \Delta f_{\text{rep}} \rangle$ -corrected frequency-comb signal. The remaining uncorrected time-dependent parameter is

the carrier-envelope offset frequency ($f_{\text{ceo}}(t)$) and hence a phase ($\phi_{\text{ceo}}(t)$). The $\phi_{\text{ceo}}(t)$ can be extracted from one of the filtered modes by computing the analytical signal. The resulting instantaneous frequency, $f_{\text{ceo}}(t) = [1/(2\pi)]d\phi_{\text{ceo}}(t)/dt$, is shown in Fig. 4(d). Applying the phase correction to the entire signal,

$$\tilde{E}_s(t) = E_s^c(t)e^{i\phi_{\text{ceo}}(t)}, \quad (5)$$

and taking into account that, for our measurements, we are in scenario II in Figs. 2(f) and 2(g), we can reconstruct the time-resolved electric field [Fig. 5(a)].

At this point we would like to mention that the signal reconstruction is based on the CoCoA algorithm represented in Ref. [14]. Namely, we have employed a digital narrow bandpass filter with zero-phase filtering, which preserves the phase of each individual mode. In this work we focus on the strongest mode in the spectrum and perform

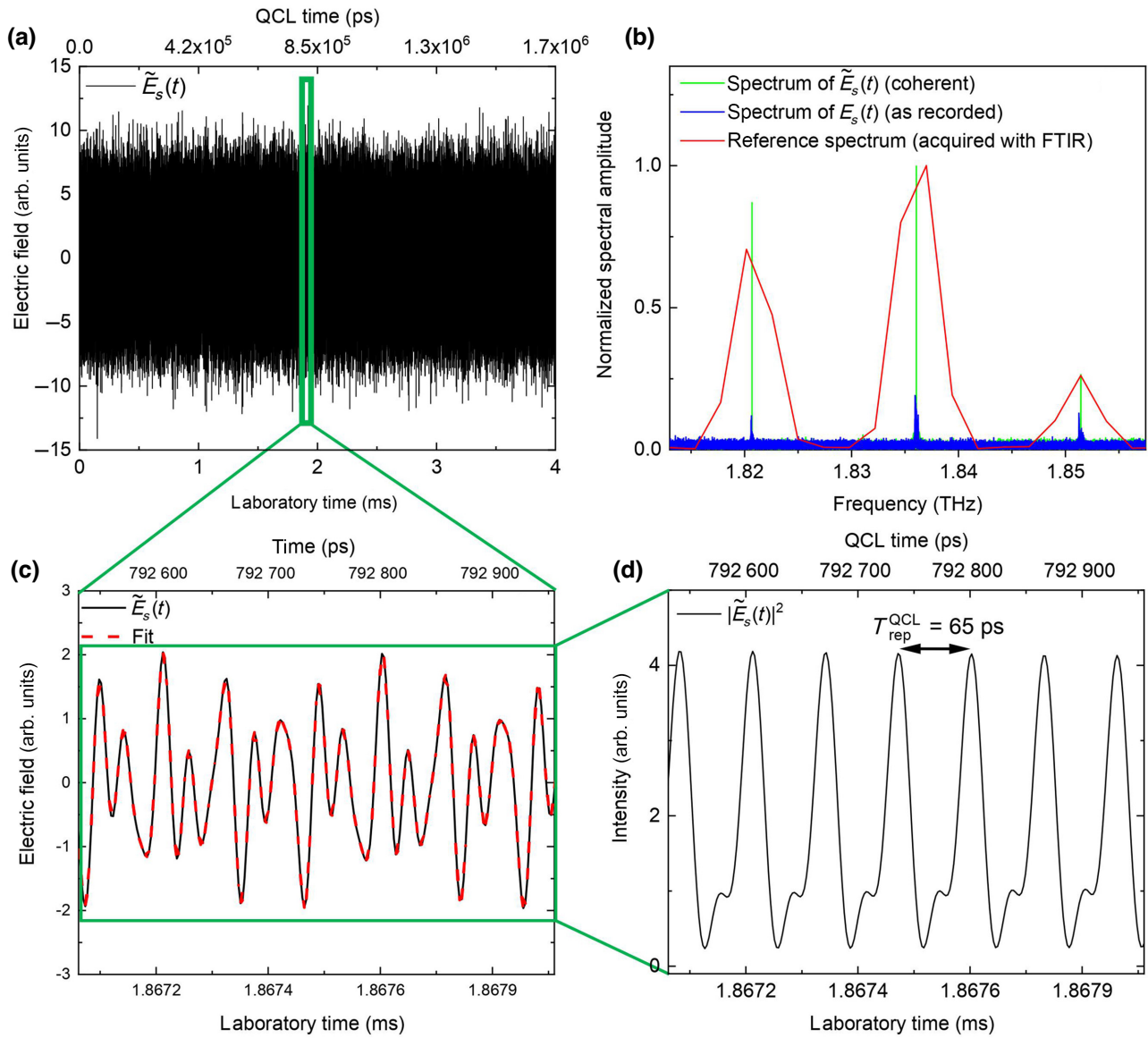


FIG. 5. (a) Phase-corrected time-resolved electric field ($\tilde{E}_s(t)$) signal of the terahertz QCL. (b) QCL spectrum of the uncorrected (blue curve, $E_s(t)$), corrected (black curve, $\tilde{E}_s(t)$) dual-comb signal, and the FT spectrometer spectrum for reference. (c) Enlarged view of (a) to show the electric field profile (black curve) and the corresponding fit. From the fit, we extract the following comb parameters: $A_1 = 7.7$, $A_2 = 9.7$, $A_3 = 4.9$, and $\Delta f_{\text{rep}} = 6.528 \text{ MHz}$, $\Delta\phi_{21} = 1.17 \text{ rad}$. (d) Computed intensity of (c) which shows a periodicity at the repetition rate of 65 ps. The time axis in the QCL reference frame was computed by applying a compression factor ($f_{\text{rep}}^{\text{fs}}/f_{\text{rep}}^{\text{QCL}}$) to the laboratory time with $f_{\text{rep}}^{\text{QCL}} = 15.377048 \text{ GHz}$ and $f_{\text{rep}}^{\text{fs}} = 79.640003 \text{ MHz}$.

the f_{ceo} correction with it. In general, performing reconstruction on weaker signals might influence the results due to the noise around the mode. However, in the case of a flat spectrum with weak modes, which we do not have here, one would rather perform the f_{ceo} correction on the average extracted phase, since the noise is uncorrelated.

Figure 5(b) shows a comparison between uncorrected (blue curve) and corrected (green curve) terahertz QCL spectra, as well the spectrum obtained with the commercial FT spectrometer (red curve). Since the mode spacing

is 6.528 MHz, we filter the modes with the narrow bandpass filter and minimize the noise which would contribute to the signal in the time domain. An enlarged view of a filtered time trace $\tilde{E}_s(t)$ is shown in Fig. 5(c) (black curve). Since the electric field signal consists of three well-defined frequencies and amplitudes, we fit the time trace and extract the amplitudes and phase differences, which are $A_1 = 7.7$, $A_2 = 9.7$, $A_3 = 4.9$, and $\Delta f_{\text{rep}} = 6.528 \text{ MHz}$, $\Delta\phi_{21} = 1.17 \text{ rad}$, $\Delta\phi_{32} = -0.54$. The corresponding fit of the electric field is shown in Fig. 5(c) as a dashed red

line, which fits well the experimental data. From the reconstructed electric field we compute the intensity $|\tilde{E}_s(t)|^2$, which is shown in Fig. 5(d). We clearly identify the round-trip time $T_{\text{rep}}^{\text{QCL}} \approx 65$ ps, in close agreement with the expected value for the QCL cavity length of 2.7 mm. In Fig. 5(d) we observe a strong amplitude-modulated comb emission. However, we relate this to the presence of two strong and one weak modes and would expect such a strong amplitude-modulated signal for our signal.

III. CONCLUSION

In conclusion, we have demonstrated EO sampling of a free-running terahertz QCL frequency comb and reconstructed the temporal electric field profile of the terahertz QCL. The reconstruction of the recorded $E_s(t)$ signal was possible, even though the initial SNR was below 10 for two of the three modes. The SNR of the EO signal is proportional to the terahertz field strength and to the square root of the NIR laser power on the balanced photodetector. Improving the SNR further could be achieved by an optimization of the data acquisition chain such that the effective integration time could be increased from the present 4 ms to minutes or even hours as is done now in dual-comb spectrometers [44]. Furthermore, implementing a high-power balanced photodetector would enable further SNR improvement at a fixed integration time.

In contrast to Ref. [41], where a QCL with single-plasmon waveguide is employed with several tens of milliwatts output power, in our case it is on the sub-milliwatt level due to the metal-metal waveguide. In the case where a metal-metal waveguide is employed, not only does a low outcoupling efficiency have to be overcome, but polarization-preserving and efficient broadband outcoupling has to be engineered. Several approaches, such as broadband antipodal Vivaldi [45], patch array antennas [46], and modified outcoupling QCL section [47], have been successfully demonstrated. Taking the above-mentioned considerations into account, we strongly believe that this technique has a high potential for investigation of weak terahertz signals, typical for ring terahertz QCL frequency combs [48], with the goal to experimentally validate possible soliton formation in a ring terahertz QCL as has been predicted by simulations in Ref. [48]. Moreover, this technique can be utilized to provide verification of engineered dispersion-compensated waveguides.

FUNDING

The authors gratefully acknowledge financial support from the European Union for research and innovation program Horizon 2020 under Grant No. 766719-FLASH Project and the ERC Grant CHIC (No. 724344).

ACKNOWLEDGMENTS

S.M. would like to acknowledge Martin Frankié for reading the manuscript, valuable suggestions, and fruitful discussions. S.M. also thanks Andres Forrer for discussions.

- [1] P. Täschler, M. Bertrand, B. Schneider, M. Singleton, P. Jouy, F. Kapsalidis, M. Beck, and J. Faist, Femtosecond pulses from a mid-infrared quantum cascade laser, *Nat. Photon.* **15**, 919 (2021).
- [2] B. Meng, M. Singleton, J. Hillbrand, M. Franckié, M. Beck, and J. Faist, Dissipative Kerr solitons in semiconductor ring lasers, *Nat. Photon.* **16**, 142 (2022).
- [3] P. Micheletti, U. Senica, A. Forrer, S. Cibella, G. Torrioli, M. Frankié, J. Faist, M. Beck, and G. Scalari, Thz optical solitons from dispersion-compensated antenna-coupled planarized ring quantum cascade lasers. ArXiv e-prints (2022), [ArXiv:2211.07242](#).
- [4] N. Picqué and T. W. Hänsch, Frequency comb spectroscopy, *Nat. Photon.* **13**, 146 (2019).
- [5] I. Coddington, N. Newbury, and W. Swann, Dual-comb spectroscopy, *Optica* **3**, 414 (2016).
- [6] A. Hugi, G. Villares, S. Blaser, H. C. Liu, and J. Faist, Mid-infrared frequency comb based on a quantum cascade laser, *Nature* **492**, 229 (2012).
- [7] S. Bartalini, L. Consolino, P. Cancio, P. De Natale, P. Bartolini, A. Taschin, M. De Pas, H. Beere, D. Ritchie, M. S. Vitiello, and R. Torre, Frequency-Comb-Assisted Terahertz Quantum Cascade Laser Spectroscopy, *Phys. Rev. X* **4**, 021006 (2014).
- [8] Z. Li, W. Wan, K. Zhou, X. Liao, S. Yang, Z. Fu, J. C. Cao, and H. Li, On-Chip Dual-Comb Source Based on Terahertz Quantum Cascade Lasers Under Microwave Double Injection, *Phys. Rev. Appl.* **12**, 044068 (2019).
- [9] F. Cappelli, L. Consolino, G. Campo, I. Galli, D. Mazzotti, A. Campa, M. Siciliani de Cumis, P. Cancio Pastor, R. Eramo, M. Rösch, M. Beck, G. Scalari, J. Faist, P. De Natale, and S. Bartalini, Retrieval of phase relation and emission profile of quantum cascade laser frequency combs, *Nat. Photon.* **13**, 562 (2019).
- [10] L. Consolino, M. Nafa, F. Cappelli, K. Garrasi, F. P. Mezzapesa, L. Li, A. G. Davies, E. H. Linfield, M. S. Vitiello, P. De Natale, and S. Bartalini, Fully phase-stabilized quantum cascade laser frequency comb, *Nat. Commun.* **10**, 2938 (2019).
- [11] C. Sirtori, S. Barbieri, and R. Colombelli, Wave engineering with THz quantum cascade lasers, *Nat. Photon.* **7**, 691 (2013).
- [12] D. Burghoff, Y. Yang, and Q. Hu, Computational multi-heterodyne spectroscopy, *Sci. Adv.* **2**, 1601227 (2016).
- [13] D. Burghoff, N. Han, and J. H. Shin, Generalized method for the computational phase correction of arbitrary dual comb signals, *Opt. Lett.* **44**, 2966 (2019).
- [14] L. A. Sterczewski, L. A. Sterczewski, L. A. Sterczewski, J. Westberg, and G. Wysocki, Computational coherent averaging for free-running dual-comb spectroscopy, *Opt. Express* **27**, 23875 (2019).

- [15] G. Brajato, L. Lundberg, V. Torres-Company, M. Karlsson, and D. Zibar, Bayesian filtering framework for noise characterization of frequency combs, *Opt. Express* **28**, 13949 (2020).
- [16] D. Burghoff, Y. Yang, D. J. Hayton, J.-R. Gao, J. L. Reno, and Q. Hu, Evaluating the coherence and time-domain profile of quantum cascade laser frequency combs, *Opt. Express* **23**, 1190 (2015).
- [17] D. Burghoff, T.-Y. Kao, N. Han, C. W. I. Chan, X. Cai, Y. Yang, D. J. Hayton, J.-R. Gao, J. L. Reno, and Q. Hu, Terahertz laser frequency combs, *Nat. Photon.* **8**, 462 (2014).
- [18] F. Cappelli, G. Villares, S. Riedi, and J. Faist, Intrinsic linewidth of quantum cascade laser frequency combs, *Optica* **2**, 836 (2015).
- [19] S. Markmann, M. Frankié, M. Bertrand, M. Shahmohammadi, A. Forrer, P. Jouy, M. Beck, J. Faist, and G. Scalari, Frequency chirped Fourier-transform spectroscopy, *Commun. Phys.* **6**, 53 (2023).
- [20] J. A. Valdmanis, G. Mourou, and C. W. Gabel, Picosecond electro-optic sampling system, *Appl. Phys. Lett.* **41**, 211 (1982).
- [21] D. Oustinov, N. Jukam, R. Rungsawang, J. Madéo, S. Barbieri, P. Filloux, C. Sirtori, X. Marcadet, J. Tignon, and S. Dhillon, Phase seeding of a terahertz quantum cascade laser, *Nat. Commun.* **1**, 69 (2010).
- [22] S. Barbieri, P. Gellie, G. Santarelli, L. Ding, W. Maineult, C. Sirtori, R. Colombelli, H. Beere, and D. Ritchie, Phase-locking of a 2.7-THz quantum cascade laser to a mode-locked erbium-doped fibre laser, *Nat. Photon.* **4**, 636 (2010).
- [23] D. R. Bacon, J. Madéo, and K. M. Dani, Photoconductive emitters for pulsed terahertz generation, *J. Opt.* **23**, 064001 (2021).
- [24] D. Burghoff, T.-Y. Kao, D. Ban, A. W. M. Lee, Q. Hu, and J. Reno, A terahertz pulse emitter monolithically integrated with a quantum cascade laser, *Appl. Phys. Lett.* **98**, 061112 (2011).
- [25] T. Seifert, *et al.*, Efficient metallic spintronic emitters of ultrabroadband terahertz radiation, *Nat. Photon.* **10**, 483 (2016).
- [26] J. Hawecker, E. Rongione, A. Markou, S. Krishnia, F. Godel, S. Collin, R. Lebrun, J. Tignon, J. Mangeney, T. Boulier, J.-M. George, C. Felser, H. Jaffrè, and S. Dhillon, Spintronic THz emitters based on transition metals and semi-metals/Pt multilayers, *Appl. Phys. Lett.* **120**, 122406 (2022).
- [27] N. Nilforoushan, T. Apretna, C. Song, T. Boulier, J. Tignon, S. Dhillon, M. Hanna, and J. Mangeney, Ultra-broadband THz pulses with electric field amplitude exceeding 100 kV/cm at a 200 kHz repetition rate, *Opt. Express* **30**, 15556 (2022).
- [28] A. Herter, A. Shams-Ansari, F. F. Settembrini, H. K. Warner, J. Faist, M. Lončar, and I.-C. Benea-Chelmus, Terahertz waveform synthesis from integrated lithium niobate circuits. (2022), [ArXiv:2204.11725](https://arxiv.org/abs/2204.11725). Accessed 2022-05-03.
- [29] J. Maysonnave, K. Maussang, J. R. Freeman, N. Jukam, J. Madéo, P. Cavalié, R. Rungsawang, S. P. Khanna, E. H. Linfield, A. G. Davies, H. E. Beere, D. A. Ritchie, S. S. Dhillon, and J. Tignon, Mode-locking of a terahertz laser by direct phase synchronization, *Opt. Express* **20**, 20855 (2012).
- [30] J. Maysonnave, N. Jukam, M. S. M. Ibrahim, R. Rungsawang, K. Maussang, J. Madéo, P. Cavalié, P. Dean, S. P. Khanna, D. P. Steenson, E. H. Linfield, A. G. Davies, S. S. Dhillon, and J. Tignon, Measuring the sampling coherence of a terahertz quantum cascade laser, *Opt. Express* **20**, 16662 (2012).
- [31] N. Jukam, S. S. Dhillon, D. Oustinov, J. Madeo, C. Manquest, S. Barbieri, C. Sirtori, S. P. Khanna, E. H. Linfield, A. G. Davies, and J. Tignon, Terahertz amplifier based on gain switching in a quantum cascade laser, *Nat. Photon.* **3**, 715 (2009).
- [32] H. Nong, S. Pal, S. Markmann, N. Hekmat, R. A. Mohandas, P. Dean, L. Li, E. H. Linfield, A. Giles Davies, and A. D. Wieck, Narrow-band injection seeding of a terahertz frequency quantum cascade laser: Selection and suppression of longitudinal modes, *Appl. Phys. Lett.* **105**, 111113 (2014).
- [33] S. Markmann, H. Nong, S. Pal, N. Hekmat, S. Scholz, N. Kukharchyk, A. Ludwig, S. Dhillon, J. Tignon, X. Marcadet, C. Bock, U. Kunze, A. D. Wieck, and N. Jukam, Spectral modification of the laser emission of a terahertz quantum cascade laser induced by broad-band double pulse injection seeding, *Appl. Phys. Lett.* **107**, 111103 (2015).
- [34] D. R. Bacon, J. R. Freeman, R. A. Mohandas, L. Li, E. H. Linfield, A. G. Davies, and P. Dean, Gain recovery time in a terahertz quantum cascade laser, *Appl. Phys. Lett.* **108**, 081104 (2016).
- [35] S. Markmann, H. Nong, S. Pal, T. Fobbe, N. Hekmat, R. A. Mohandas, P. Dean, L. Li, E. H. Linfield, and A. G. Davies, Two-dimensional coherent spectroscopy of a THz quantum cascade laser: Observation of multiple harmonics, *Opt. Express* **25**, 21753 (2017).
- [36] J. Riepl, J. Raab, P. Abajyan, H. Nong, J. R. Freeman, L. H. Li, E. H. Linfield, A. G. Davies, A. Wacker, T. Albes, C. Jirauschek, C. Lange, S. S. Dhillon, and R. Huber, Field-resolved high-order sub-cycle nonlinearities in a terahertz semiconductor laser, *Light: Sci. Appl.* **10**, 246 (2021).
- [37] S. Markmann, M. Franckié, S. Pal, D. Stark, M. Beck, M. Fiebig, G. Scalari, and J. Faist, Two-dimensional spectroscopy on a THz quantum cascade structure, *Nanophotonics* **10**, 171 (2021).
- [38] F. Wang, H. Nong, T. Fobbe, V. Pistore, S. Houver, S. Markmann, N. Jukam, M. Amanti, C. Sirtori, S. Moumdji, R. Colombelli, L. Li, E. Linfield, G. Davies, J. Mangeney, J. Tignon, and S. Dhillon, Short terahertz pulse generation from a dispersion compensated modelocked semiconductor laser, *Laser Photon. Rev.* **11**, 1700013 (2017).
- [39] P. Gellie, S. Barbieri, J.-F. Lampin, P. Filloux, C. Manquest, C. Sirtori, I. Sagnes, S. P. Khanna, E. H. Linfield, A. G. Davies, H. Beere, and D. Ritchie, Injection-locking of terahertz quantum cascade lasers up to 35 GHz using RF amplitude modulation, *Opt. Express* **18**, 20799 (2010).
- [40] L. Consolino, A. Taschin, P. Bartolini, S. Bartalini, P. Cancio, A. Tredicucci, H. E. Beere, D. A. Ritchie, R. Torre, M. S. Vitiello, and P. De Natale, Phase-locking to a free-space terahertz comb for metrological-grade terahertz lasers, *Nat. Commun.* **3**, 1040 (2012).

- [41] S. Barbieri, M. Ravaro, P. Gellie, G. Santarelli, C. Manquest, C. Sirtori, S. P. Khanna, E. H. Linfield, and A. G. Davies, Coherent sampling of active mode-locked terahertz quantum cascade lasers and frequency synthesis, *Nat. Photon.* **5**, 306 (2011).
- [42] G. Gallot and D. Grischkowsky, Electro-optic detection of terahertz radiation, *JOSA B* **16**, 1204 (1999).
- [43] O. Kliebisch, D. C. Heinecke, S. Barbieri, G. Santarelli, H. Li, C. Sirtori, and T. Dekorsy, Unambiguous real-time terahertz frequency metrology using dual 10 GHz femtosecond frequency combs, *Optica* **5**, 1431 (2018).
- [44] K. Komagata, A. Shehzad, G. Terrasanta, P. Brochard, R. Matthey, M. Gianella, P. Jouy, F. Kapsalidis, M. Shahmohammadi, M. Beck, V. J. Wittwer, J. Faist, L. Emmenegger, T. Südmeyer, A. Hugi, and S. Schilt, Coherently-averaged dual comb spectrometer at $7.7 \mu\text{m}$ with master and follower quantum cascade lasers, *Opt. Express* **29**, 19126 (2021).
- [45] U. Senica, E. Mavrona, T. Olariu, A. Forrer, M. Shahmohammadi, M. Beck, J. Faist, and G. Scalari, An antipodal Vivaldi antenna for improved far-field properties and polarization manipulation of broadband terahertz quantum cascade lasers, *Appl. Phys. Lett.* **116**, 161105 (2020).
- [46] L. Bosco, C. Bonzon, K. Ohtani, M. Justen, M. Beck, and J. Faist, A patch-array antenna single-mode low electrical dissipation continuous wave terahertz quantum cascade laser, *Appl. Phys. Lett.* **109**, 201103 (2016).
- [47] T. Fobbe, H. Nong, R. Schott, S. Pal, S. Markmann, N. Hekmat, J. Zhu, Y. Han, L. Li, P. Dean, E. H. Linfield, A. G. Davies, A. D. Wieck, and N. Jukam, Improving the out-coupling of a metal-metal terahertz frequency quantum cascade laser through integration of a hybrid mode section into the waveguide, *J. Infrared, Millimeter, Terahertz Waves* **37**, 426 (2016).
- [48] M. Jaidl, *et al.*, Comb operation in terahertz quantum cascade ring lasers, *Optica* **8**, 780 (2021).